

A Novel Shoulder Exoskeleton Robot Using Parallel Actuation and a Passive Slip Interface

Justin Hunt¹

School for Engineering of Matter,
Transport and Energy,
Arizona State University,
Tempe, AZ 85287
e-mail: justin.p.hunt@asu.edu

Hyunglae Lee

School for Engineering of Matter,
Transport and Energy,
Arizona State University,
Tempe, AZ 85287
e-mail: hyunglae.lee@asu.edu

Panagiotis Artemiadis

School for Engineering of Matter,
Transport and Energy,
Arizona State University,
Tempe, AZ 85287
e-mail: panagiotis.artemiadis@asu.edu

This paper presents a five degrees-of-freedom (DoF) low inertia shoulder exoskeleton. This device is comprised of two novel technologies. The first is 3DoF spherical parallel manipulator (SPM), which was developed using a new method of parallel manipulator design. This method involves mechanically coupling certain DoF of each independently actuated linkage of the parallel manipulator in order to constrain the kinematics of the entire system. The second is a 2DoF passive slip interface used to couple the user upper arm to the SPM. This slip interface increases system mobility and prevents joint misalignment caused by the translational motion of the user's glenohumeral joint from introducing mechanical interference. An experiment to validate the kinematics of the SPM was performed using motion capture. The results of this experiment validated the SPM's forward and inverse kinematic solutions through an Euler angle comparison of the actual and command orientations. A computational slip model was created to quantify the passive slip interface response for different conditions of joint misalignment. In addition to offering a low inertia solution for the rehabilitation or augmentation of the human shoulder, this device demonstrates a new method of motion coupling, which can be used to impose kinematic constraints on a wide variety of parallel architectures. Furthermore, the presented device demonstrates a passive slip interface that can be used with either parallel or serial robotic systems. [DOI: 10.1115/1.4035087]

1 Introduction

A parallel manipulator is a robotic mechanism that uses multiple actuated parallel linkages to synergistically manipulate the motion of its end effector. The architecture of these devices can vary considerably, but usually consists of between two and six rotational or linear actuators, which couple a mobile platform to a stationary base. In comparison to the more common serial chain manipulator, parallel manipulators typically offer better end-effector performance in terms of precision, velocity, and torque generation [1–3]. Parallel manipulators also tend to exhibit lower effective inertia than serial chain manipulators [3,4]. Furthermore, it is possible to design a parallel manipulator such that it does not occupy its center of rotation. This unique combination of advantages, inherent to parallel manipulation, suggests that this type of robotic architecture would be suitable for exoskeleton limb applications.

Parallel manipulators have been used for several exoskeleton applications. Prior works include wearable wrist [5], ankle [6], and shoulder [7] devices. All of these demonstrate different types of parallel architecture. The RiceWrist [5] uses a three-RPS (revolute–prismatic–spherical) manipulator with an additional serial revolute joint to generate four degrees-of-freedom (DoF) that includes the rotation of the forearm, wrist height, and 2DoF in rotation of the end-effector platform. The Anklebot [6] uses a two-SPS-1S (spherical–prismatic–spherical, spherical) manipulator that consists of spherical joints and prismatic actuation in conjunction with the biological joint to achieve spherical motion. The shoulder exoskeleton BONES [7] uses an RRPS (revolute–revolute–prismatic–spherical) manipulator to decouple and control three rotational DoF. Because all of these devices generate spherical motion through parallel actuation, they can further be categorized as spherical parallel manipulators (SPMs).

The prior works [5,6] focus on biological joints that can be modeled as either having purely rotational or spherical motion.

Although this simplifying assumption is a good approximation for these joints, it has demonstrated inaccuracy for more complex joints like the shoulder. Rotational motion of the shoulder's clavicle and scapula results in translational motion of the glenohumeral joint [8,9]. Therefore, the humerus of the upper arm actually has both rotational and translational motion. This has been realized by previous works [10–14] whom have all built serial actuated shoulder exoskeletons to more accurately emulate the shoulder's motion by incorporating translational DoF into their designs. However, the choice of using serial actuation has the inherent disadvantages of low stiffness, high inertia, and positioning errors that are accumulated and amplified from base to end effector.

A solution for emulating the complex rotational and translational motion of the shoulder might be to use a parallel manipulator with a higher degree of actuation. A possibility would be the six linear actuator “hexapod” design known as the Gough–Stewart (GS) platform [15]. This device has control over all 6DoF of its platform and exhibits good stiffness characteristics, making it ideal for high precision and high load applications. However, the GS platform has limited workspace. This is due largely in part to mechanical interference between the device's many parallel linkages. Designing a GS platform with the same range of motion as the shoulder would be difficult [16,17]. In addition, the argument could be made that a fully actuated 6DoF system is an overly complicated solution to address the relatively small degree of translational motion of the shoulder.

An alternative to using a more complicated 4, 5, or 6DoF controlled parallel manipulator is to use a 3DoF SPM with an integrated passive slip interface. Allowing slip to occur between user and device could be used to alleviate mechanical interference associated with joint misalignment. This mechanical interference could otherwise induce dangerous forces on the user and may also introduce errors in the parallel manipulator kinematics as a result of reaction forces applied by the user [18]. The use of passive slip also simplifies the control scheme of the parallel manipulator, since the degree of joint misalignment no longer needs to be quantified and accounted for. Slip interfaces have been utilized in the works [19–21], all of which have identified it as a viable means of preventing mechanical interference.

¹Corresponding author.

Manuscript received May 23, 2016; final manuscript received October 19, 2016; published online November 23, 2016. Assoc. Editor: Jun Ueda.

With the exception of BONES, incorporating slip into current SPM designs would be difficult for a shoulder exoskeleton application. The RRPS architecture used with BONES could be modified to include a slip mechanism. However, BONES uses four linear actuators to control the 3DoF of the shoulder, whereas other SPM architectures have shown that it is possible to achieve 3DoF control with only three actuators [22]. The two-SPS design in Ref. [6] uses the biological joint as part of the kinematic solution and will not work with slip. One SPM possibility would be the three-RRR (rotational–rotational–rotational) “Agile Eye” parallel manipulator. This device uses three rotary actuators and curved linkages to decouple and control the three rotational DoF [22,23]. However, the three-RRR’s architecture does not interface well with the human shoulder, as its curved linkages pass through the majority of the sphere in which it rotates about. This would cause interference between the user and device. Another SPM possibility would be the three-UPU (universal–prismatic–universal) “Spherical Wrist” parallel manipulator. This SPM consists of three parallel linear actuators, which decouple and control the three rotational DoF [22,24]. The use of only three linear actuators introduces minimal mechanical interference and results in a large workspace compared to other SPMs [25]. Additionally, the three-UPU design is compact, which is advantageous for mobile applications. However, the three-UPU has been shown to exhibit poor stiffness characteristics, which makes it impractical for real world use [26].

In order to address this lack of compatibility with current SPMs and the proposed method of slip, a novel parallel manipulator has been developed. This parallel manipulator shares the SPS characteristic of spherical platform mounting joints and the three-UPU characteristic of universal base mounting joints, but uses a novel method of coupling certain motions of each actuator independently in order to produce a device with a single kinematic solution.

The rest of this paper presents this novel SPM design along with the discussed slip mechanism for handling translational motion of the shoulder. The sections are organized as follows: Sec. 2 details the design of the SPM and slip mechanism. Section 3 details the results of an experiment to validate the kinematics and workspace. Finally, Sec. 4 concludes the paper with a discussion and summary of the contribution.

2 Methods

2.1 Design Overview. The developed SPM is presented in Fig. 1. The device weighs 5.4 kg, excluding batteries and off-board controller. It consists of three parallel linear actuators connected to a shoulder piece coupled to the user. Each actuator has 3DoF. Two of the DoF are rotational (roll and pitch) and one is translational (stroke). The roll of each actuator is defined to rotate about the vector connecting the actuator’s base mounting point to the center of rotation of the user’s shoulder. The roll is not directly constrained, but rather set by the synergistic movements of all three actuators. The pitch and length of each actuator are mechanically coupled such that the workspace is a spherical surface centered about the user’s shoulder. Each actuator is connected to the shoulder piece by a 3DoF tie-rod joint. The shoulder piece is connected to the user’s arm by a 2DoF passive slip joint that allows for 1DoF of rotational motion and 1DoF of translational motion. The rotational DoF prevents undesired torques from being applied to the user’s arm during the rolling action of the exoskeleton shoulder. The translational DoF allows slip to occur between the user and the device. The base mounts of each actuator are situated in close proximity to the user’s back. However, placement of the base mounts is flexible and only limited by physical constraints, such as mechanical interference. Several viable alternative mounting configurations are shown in Fig. 2.

2.2 Actuator Motion Coupling. One of the primary features of this SPM is that it uses the novel method of motion coupling to



Fig. 1 The SPM design. Conceptual model illustrating interface with user (top). Prototype (bottom).

produce a device with a single kinematic solution. This method involves coupling certain DoF of each actuator independently in order to constrain the multiple kinematic solutions of the non-coupled system to a single solution for the coupled system. For this SPM, the pitch angle θ and length vector \vec{L} of each independent actuator are coupled such that all possible kinematic solutions lie on a sphere centered about the user’s shoulder C . With reference to Fig. 3, the desired θ is

$$\theta = a \tan 2(L_y, L_x) \quad (1)$$

where $atan2$ is a quadrant corrected arctangent function. In order to achieve this required θ angle, a linear slider mounted near the actuator base B of the actuator is used. This slider controls the position of armature vector \vec{r} along \vec{L} and is driven by the same motor that drives \vec{L} , but with a different gearing ratio. Instead of

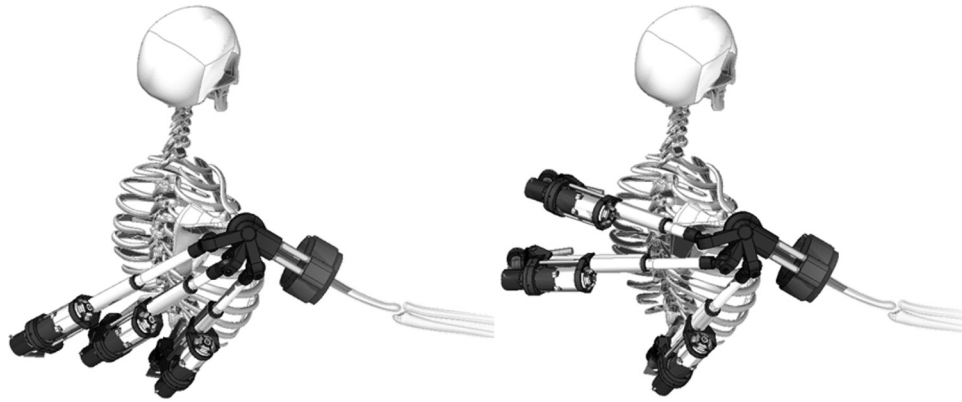


Fig. 2 Examples of alternative base mount configurations

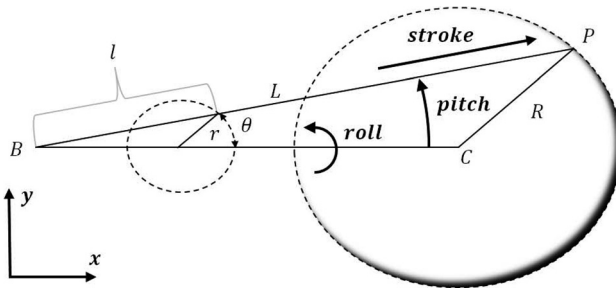


Fig. 3 Actuator pitch and stroke coupling using similar triangle relation

solving the nonlinear Eq. (1) for θ , it is possible to solve for the slider distance vector \bar{l} along \bar{L} , which is described by a similar triangle relationship between B , C , and the mobile platform mount P . This same relationship can also be expressed in scalar terms as

$$\|\bar{l}\| = \frac{\|\bar{L}\|\|\bar{r}\|}{\|\bar{R}\|} \quad (2)$$

In practice, however, it was found that the similar triangle relationship between lrd and LRD is difficult to maintain. An offset vector \bar{o} from B is necessary to avoid mechanical interference. As shown in Fig. 4, the existence of \bar{o} also introduces an offset vector \bar{h} between \bar{r} and \bar{d} . Solutions for \bar{r} , \bar{h} , and \bar{d} can be found by fitting an arc to three slider positions \bar{p} that correspond to three

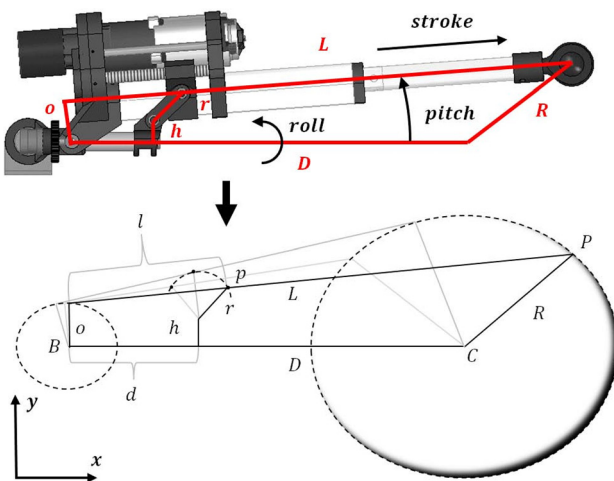


Fig. 4 Actuator pitch and stroke coupling with offsets r' and d' to avoid mechanical interference

arbitrary values of \bar{L} that exist on the desired spherical workspace. The center of the arc represents the position $\bar{d} + \bar{h}$ and the arc radius represents \bar{r} . To construct the arc, the vector components o_x , o_y , L_x , and L_y must first be solved. This can be achieved by the following system of vector and trigonometric equations with relation to the known terms $\|\bar{o}\|$, D , and \bar{R} :

$$\bar{o} + \bar{L} = \bar{D} + \bar{R} \quad (3)$$

$$\|\bar{o}\|^2 = o_x^2 + o_y^2 \quad (4)$$

$$\|\bar{o}\|^2 + L_x^2 + L_y^2 = (R_x + D_x)^2 + (R_y + D_y)^2 \quad (5)$$

where Eq. (3) is the vector relation of \bar{D} and \bar{R} to \bar{o} and \bar{L} . The trigonometric Eqs. (4) and (5) relate the known magnitude $\|\bar{o}\|$ and the right angle relation of \bar{o} and \bar{L} to the unknown vectors components of \bar{o} and \bar{L} .

With the components of \bar{L} and \bar{o} known, it is possible to solve for the slider distance vector \bar{l} along \bar{L} , which is necessary in order to determine the slider position vector \bar{p} with respect to B . The vector \bar{l} is a function of the collinear vector \bar{L} and the design choices of slider offset l_o from \bar{o} , gear ratio w , and retracted actuator length L_o . With reference to Fig. 4, this relationship can be described by

$$\bar{l} = w(\bar{L} - L_o\bar{u}) + l_o\bar{u} \quad (6)$$

where

$$\bar{u} = \frac{\bar{L}}{\|\bar{L}\|} \quad (7)$$

The slider position \bar{p} expressed as a vector from \bar{B} is

$$\bar{p} = \bar{l} + \bar{o} \quad (8)$$

Given three slider position vectors \bar{p}_1 , \bar{p}_2 , and \bar{p}_3 which correspond to three arbitrary actuator lengths \bar{L}_1 , \bar{L}_2 , and \bar{L}_3 , respectively, which exist on the spherical workspace, it is now possible to construct the arc and solve for \bar{r} , \bar{h} , and \bar{d} .

One of the motion coupled position feedback actuators is shown in Fig. 5. Each actuator has been configured such that the device operates on a spherical surface at a radius of $\|\bar{R}\| = 95.17$ mm from the center of rotation of the user's shoulder. This radius was determined through measurement of the shoulder center of rotation to the outer surface of the lateral and posterior deltoids of three adult male subjects. Given this radius, a computer model of the design was created using the CAD package Solid Edge. This model allows the required maximum stroke length of each actuator to be solved given the chosen mounting point and desired

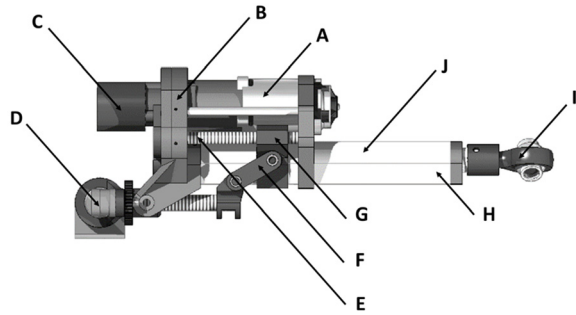


Fig. 5 Motion coupled actuator. Conceptual model (top) with the following components: (A) motor, (B) custom gearbox, (C) pitch/stroke encoder, (D) roll measurement potentiometer, (E) wormscrew, (F) pitch/stroke coupling linkage, (G) pitch control slider, (H) enclosed limit switches, (I) tie rod joint, and (J) enclosed powerscrew and slider for linear actuation. Developed prototype (bottom).

workspace. The mounting points of the top, middle, and bottom actuator with respect to the global frame shown in Fig. 6 are $[-33, -10, 19]$ cm, $[-28, -17, -20]$ cm, and $[-10, -12, -24]$ cm, respectively. Each actuator mount is fixed to an external scaffold built from strut channel. The workspace of this shoulder exoskeleton was chosen to be one octant of a sphere. Given these conditions and the industry available sizes, the maximum stroke lengths were decided at 152.42 mm for the top and middle actuator and 101.62 mm for the bottom actuator.

2.3 Inverse Kinematics. For the global frame defined in Fig. 6, the inverse kinematic solution can be determined by first

defining the local frame vector \bar{x}' to be collinear to the user's desired arm direction. The direction of the user's arm is defined by the vector between the glenohumeral joint and the elbow. The vector \bar{x}' can be further described by the spherical coordinate inclination angle θ and azimuth angle ϕ , which are defined in Fig. 6. The initial orientation of the local vector \bar{z}' can be expressed as the cross products of \bar{x}' and the global vector \bar{z} . The local vector \bar{y}' is the cross product of \bar{z}' and \bar{x}' . It is necessary to multiply this initial set of orientation vectors, represented by R' in column form, by a rotation matrix R_x about \bar{x}' in order to keep the shoulder within the workspace of the three linear actuators. Hence, the new rotation matrix is

$$R'' = R'R_x \quad (9)$$

where

$$R' = \begin{bmatrix} x'_x & y'_x & z'_x \\ x'_y & y'_y & z'_y \\ x'_z & y'_z & z'_z \end{bmatrix} \quad (10)$$

$$R_x = \begin{bmatrix} 1 & 0 & 0 \\ 0 & \cos \psi & -\sin \psi \\ 0 & \sin \psi & \cos \psi \end{bmatrix} \quad (11)$$

The Euler angle ψ in Eq. (11) represents the angle of rotation about \bar{x}' . Finding ψ , which determines R_x , is done by first identifying a set of key orientations that define the workspace. For this device, approximately one octant of a sphere is a decidedly sufficient workspace to demonstrate proof of concept. The chosen orientation matrices at arm rest R''_r ($\theta = -90$ deg, $\phi = 90$ deg, or $\theta = -90$ deg, $\phi = 0$ deg), arm flexion R''_f ($\theta = 0$ deg, $\phi = 90$ deg), and arm abduction R''_a ($\theta = 0$ deg, $\phi = 0$ deg) of the shoulder piece for the three corners of the octant are shown in Fig. 6. For these orientations, Eq. (9) becomes

$$R''_r = \begin{bmatrix} 0 & 0 & 1 \\ 0 & 1 & 0 \\ -1 & 0 & 0 \end{bmatrix} = \begin{bmatrix} 0 & 0 & 1 \\ 0 & 1 & 0 \\ -1 & 0 & 0 \end{bmatrix} \begin{bmatrix} 1 & 0 & 0 \\ 0 & 1 & 0 \\ 0 & 0 & 1 \end{bmatrix} \quad (12)$$

or

$$R''_r = \begin{bmatrix} 0 & 0 & 1 \\ 0 & 1 & 0 \\ -1 & 0 & 0 \end{bmatrix} = \begin{bmatrix} 0 & 1 & 0 \\ 0 & 0 & -1 \\ -1 & 0 & 0 \end{bmatrix} \begin{bmatrix} 1 & 0 & 0 \\ 0 & 0 & 1 \\ 0 & -1 & 0 \end{bmatrix} \quad (13)$$

and

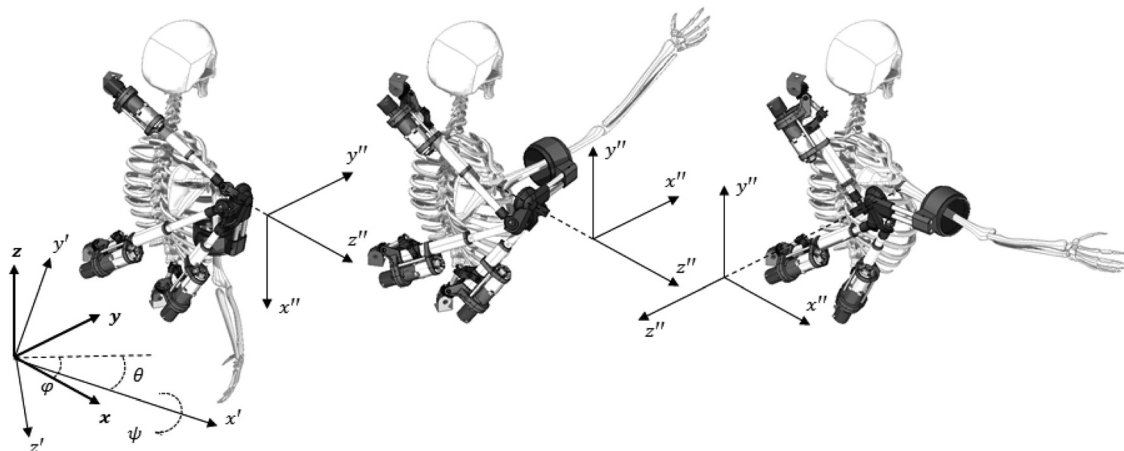


Fig. 6 Chosen exoskeleton shoulder orientation for given arm directions

$$\mathbf{R}_r'' = \begin{bmatrix} 0 & 0 & 1 \\ 1 & 0 & 0 \\ 0 & 1 & 0 \end{bmatrix} = \begin{bmatrix} 0 & 0 & 1 \\ 1 & 0 & 0 \\ 0 & 1 & 0 \end{bmatrix} \begin{bmatrix} 1 & 0 & 0 \\ 0 & 1 & 0 \\ 0 & 0 & 1 \end{bmatrix} \quad (14)$$

$$\mathbf{R}_a'' = \begin{bmatrix} 1 & 0 & 0 \\ 0 & 0 & -1 \\ 0 & 1 & 0 \end{bmatrix} = \begin{bmatrix} 1 & 0 & 0 \\ 0 & 0 & -1 \\ 0 & 1 & 0 \end{bmatrix} \begin{bmatrix} 1 & 0 & 0 \\ 0 & 1 & 0 \\ 0 & 0 & 1 \end{bmatrix} \quad (15)$$

It is important to note that the orientation of R' in Eqs. (12) and (13) cannot be achieved, since $\bar{z}' = \bar{x}' \times \bar{z}$. However, for the purpose of solving for ψ , \mathbf{R}_r can be assumed to reach this orientation. In practice, only a solution infinitesimally close to this orientation can be achieved. For \mathbf{R}_x in Eqs. (12)–(15), $\psi = 0$ deg, -90 deg, 0 deg, and 0 deg, respectively. Given ψ and the corresponding θ and ϕ , it is possible to derive a general relation using a multivariable sinusoidal fit which defines ψ for the entire workspace. The function ψ of θ and ϕ is described by

$$\psi = \sin(\theta) \left(\frac{\pi}{2} - \phi \right) \quad (16)$$

With a known orientation \mathbf{R}'' and a chosen radius of operation R , a chain of transformation matrices can then be used to describe the position of any point on the exoskeleton shoulder. For the location of an arbitrary mounting point described by \bar{P} with respect to the local exoskeleton shoulder frame at R from the center of rotation, this transformation matrix \mathbf{T} becomes

$$\mathbf{T} = \begin{bmatrix} x_x'' & y_x'' & z_x'' & z_x'' R \\ x_y'' & y_y'' & z_y'' & z_y'' R \\ x_z'' & y_z'' & z_z'' & z_z'' R \\ 0 & 0 & 0 & 1 \end{bmatrix} \begin{bmatrix} 1 & 0 & 0 & P_x \\ 0 & 1 & 0 & P_y \\ 0 & 0 & 1 & P_z \\ 0 & 0 & 0 & 1 \end{bmatrix} \quad (17)$$

where x_x'' , x_y'' , x_z'' , y_x'' , y_y'' , y_z'' , z_x'' , z_y'' , and z_z'' are the components of \mathbf{R}'' . With the location of base mounting point \bar{D} known and the platform mounts described by translational components of \mathbf{T} known, the length of each actuator L_i is the Euclidean distance between its respective mounting points

$$\|\bar{L}_i\| = \sqrt{(T_{14_i} - D_{x_i})^2 + (T_{24_i} - D_{y_i})^2 + (T_{34_i} - D_{z_i})^2} \quad (18)$$

2.4 Forward Kinematics. The forward kinematics of this SPM is solved by using position feedback sensors. Each actuator is equipped with an encoder (Karlsson Robotics E6C2), having a resolution of 1024 pulses/rotation, to record the coupled pitch and stroke length. The roll of each actuator is measured using a 10 k Ω potentiometer (Bourns 3590 S). The endpoint of each actuator is found from both angles and the stroke length. The position and orientation of the platform is found from the three actuator endpoints.

2.5 Slip Mechanism. The slip mechanism, used in this shoulder exoskeleton for preventing the adverse effects of joint misalignment, consists of a passive cuff joint with one translational DoF and one rotational DoF. The internal cuff of this joint has a compliant padded interior which is designed to stay in contact with the user's upper arm. The external cuff is connected to the shoulder exoskeleton. When joint misalignment between the center of rotation of the user's glenohumeral joint and the center of rotation of the shoulder exoskeleton occurs, the internal cuff translates within the external cuff as shown in Fig. 7. In addition to translational slip S , joint misalignment will affect the orthogonal relationship between the cross section of the external/internal cuff and the user's arm. This cuff misalignment angle ω is shown in Fig. 7. The compliance of the internal cuff's padding allows for a degree of angular misalignment to occur without harm to the user or device. The internal cuff used in this prototype permits

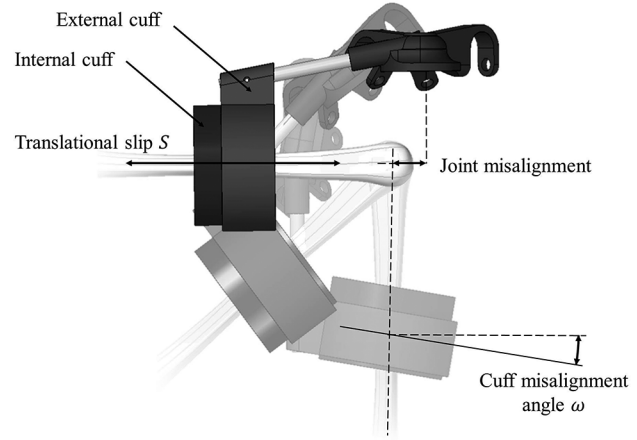


Fig. 7 Upper arm slip mechanism for joint misalignment

3 cm of diametral padding deformation. The maximum angular misalignment is a function of this allowable deformation and of the user's arm diameter.

The joint misalignment vector \bar{v}_{mis} can occur in any direction. However, the maximum translational slip S_{max} will always occur when user's arm direction vector \bar{v}_{user} is collinear to \bar{v}_{mis} , for which $\|\bar{S}_{max}\| = \|\bar{v}_{mis}\|$. This case of maximum slip is exemplified in Fig. 7 for which horizontal joint misalignment has occurred and the user arm is at a 90 deg abduction angle from the resting position. The maximum cuff misalignment angle ω_{max} is also shown in Fig. 7 and occurs at the resting position when \bar{v}_{mis} is orthogonal to \bar{v}_{user} . Both S_{max} and ω_{max} have rotational symmetry about \bar{v}_{mis} and therefore any arbitrary plane about \bar{v}_{mis} can be examined to determine \bar{S}_{max} and ω_{max} . With reference to Fig. 8, \bar{S}_{max} and ω_{max} are solved by first projecting the components of the \bar{v}_{mis} into the plane comprised of \bar{v}_{mis} , $\bar{v}_{user \perp mis}$, and $\bar{v}_{user \parallel mis}$. Using the collinear relation between \bar{v}_{user} and \bar{S} and the vector relation between \bar{v}_{user} , \bar{v}_{mis} and the shoulder exoskeleton arm vector \bar{v}_{exo} , \bar{S} can be solved by the following system:

$$\|\bar{v}_{exo}\|^2 = (v_{misxy} + S_{xy} - v_{userxy})^2 + (v_{misz} + S_z - v_{userz})^2 \quad (19)$$

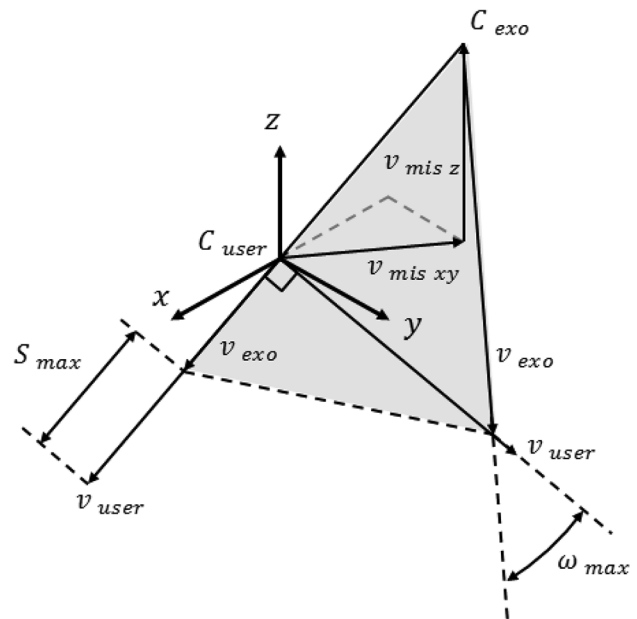


Fig. 8 Upper arm slip mechanism with joint misalignment in 3D space

$$\frac{S_{xy}}{S_z} = \frac{v_{user,xy}}{v_{user,z}} \quad (20)$$

Of the two possible solution sets, the correct set will match the sign notation of the components of \bar{v}_{user} . With \bar{S} known, ω is expressed as the angle between \bar{v}_{user} and \bar{v}_{exo} , where $\bar{v}_{exo} = \bar{v}_{mis} + \bar{v}_{user} - \bar{S}$.

2.6 Control System. To operate the shoulder exoskeleton, a keyboard control scheme running on an off-board personal computer for high-level control was used. The user commands the θ and ϕ angles in 5 deg increments using the arrow keys within a MATLAB interface. The MATLAB script solves the forward and inverse kinematics based on the user's desired position and sends new position and velocity commands via serial communication to a microcontroller (Arduino Mega 2560). This microcontroller then relays the position commands to a set of corresponding proportional-integral-derivative motion controllers (Kangaroo 2x Motion Controller), which are connected to a set of motor drivers (SyRen 10 A Regenerative Motor Driver). Each motion controller was in a feedback loop with its respective actuator's encoder and limit switches. Once the desired positions are met, a secondary feedback loop alerts MATLAB that the motion controller is ready to execute the next set of commands.

2.7 Experimental Setup. To validate the kinematics, we conducted a preliminary experiment using VICON motion capture. Three IR markers were placed on the shoulder piece and tracked by a set of four IR motion capture cameras (VICON Bonita B10) throughout a grid trajectory that varied both θ and ϕ in 5 deg increments. The ranges of θ and ϕ were determined experimentally by moving the shoulder exoskeleton until either a limit switch was triggered or mechanical interference was identified. The conservative choices of $0 \text{ deg} \leq \theta \leq -85 \text{ deg}$ and $0 \text{ deg} \leq \phi \leq 80 \text{ deg}$ were used for the experiment in order to ensure that a limit would not be reached. Both θ and ϕ are functional to the placement and maximum stroke length of each actuator. Adjusting either of these parameters will affect the workspace. The marker data were streamed to the real-time motion capture software Tracker and used to reconstruct the local frame, which was compared to the commanded orientation at each grid point. The comparison was done using z - x - z Euler angles.

To quantify the translation slip S and the cuff angular misalignment ω , a computational slip model was constructed with reference to Eqs. (19) and (20). The model uses the joint misalignment vector \bar{v}_{mis} , the user's arm direction vector \bar{v}_{user} , and a zero cuff position at 166 mm from the center of rotation as inputs. In this model, the convention chosen is that θ exists in quadrant III ($-x$, $-y$) of the plane and that positive joint misalignment exists in quadrant I ($+x$, $+y$).

3 Results

3.1 SPM Kinematics. The experiment conducted to validate the SPM kinematics using motion capture yielded the following results. The difference between the z - x - z Euler angles of the actual and command orientation, with respect to the corresponding θ and ϕ angles, is presented in Fig. 9. This figure indicates an increasing error trend toward the bounds of the workspace. The data collected shows mean Euler angle errors of $\alpha_{mean} = 1.01 \text{ deg}$, $\beta_{mean} = 0.46 \text{ deg}$, and $\gamma_{mean} = 1.87 \text{ deg}$. The variance of the Euler angles were calculated to be 1.18 deg, 0.3 deg, and 3.46 deg for α , β , and γ , respectively. The maximum Euler angle errors were recorded to be 2.15 deg, 1.42 deg, and 6.02 deg for α , β , and γ , respectively.

3.2 Slip Mechanism. The model results in Figs. 10 and 11 show S_{max} and ω_{max} , respectively, across a complete 90 deg degree variation of θ . It can be observed from Fig. 10 that S_{max} is minimized for planar joint misalignment when the joint

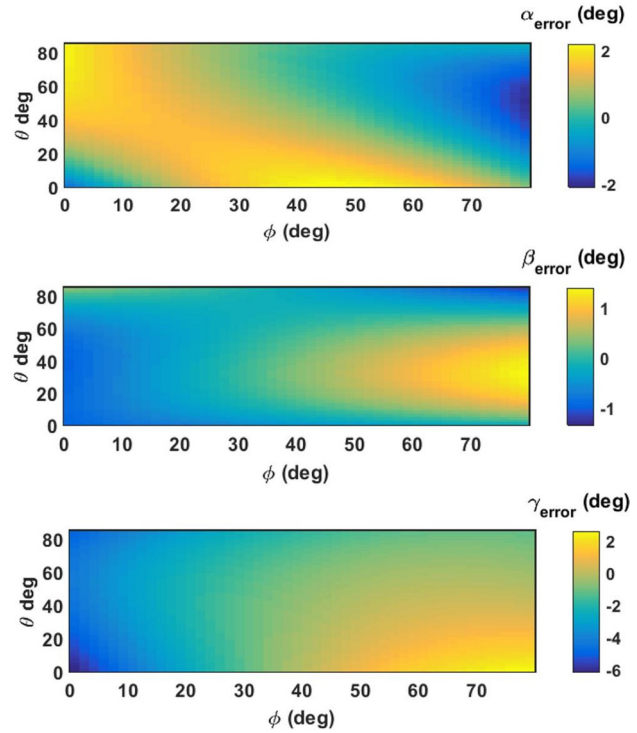


Fig. 9 Error between the actual and commanded shoulder orientation expressed using the z - x - z Euler angles α , β , and γ , respectively

misalignment vector is in the opposing direction to \bar{v}_{user} at $\theta = -45 \text{ deg}$. In Fig. 11, it can be observed that ω_{max} is minimized for planar joint misalignment when \bar{v}_{mis} is collinear to \bar{v}_{user} at $\theta = -45 \text{ deg}$. These models demonstrate that for the case study in which 5 cm of misalignment has occurred, the maximum possible slip and angular misalignment that the user could experience is $S_{max} = 5 \text{ cm}$ and $\omega_{max} = 17.16 \text{ deg}$.

4 Discussion

This paper presented a novel 5DoF shoulder exoskeleton using parallel actuation and an integrated passive slip interface. By using a parallel architecture, our system offers a low inertia solution to limb actuation, which is important with regard to energy

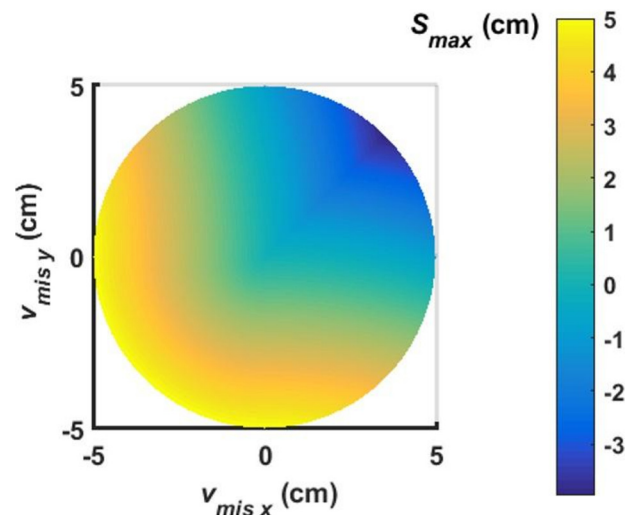


Fig. 10 Maximum translation slip S_{max} of the cuff for given planar misalignment v_{mis}

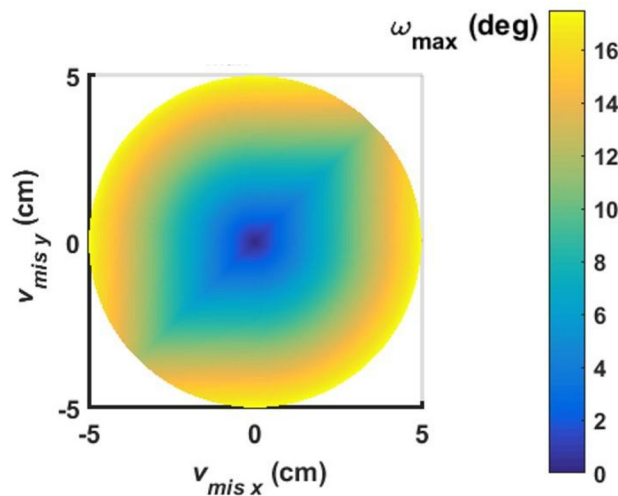


Fig. 11 Maximum cuff misalignment angle ω_{\max} for given planar misalignment v_{mis}

cost and the performance of wearable devices. We also presented the method of motion coupling that was used to develop this new type of SPM with a single kinematic solution. This method could be applied to other parallel or serial actuated architectures in order to further constrain motion. Finally, this paper discusses how the use of a slip interface can be used for negating the adverse effects of joint misalignment and how it allows the presented SPM in particular to be used to emulate the complex motion of the human shoulder. It is important to note that this idea of allowing mechanical slip could be extended to include the rest of the arm as well. For a full arm exoskeleton, a secondary slip mechanism would be necessary after the elbow joint.

An experiment was performed to validate the kinematics of the SPM using motion capture. This experiment showed mean Euler angle errors of 1.01 deg, 0.46 deg, and 1.87 deg for α , β , and γ , respectively. Contribution of error includes compliance of 3D printed materials used in the construction of the actuators, low machining tolerances associated with in-house fabrication, and a placement tolerance of 3 mm for the base mounting brackets. Additionally, a computational model to simulate the maximum translation slip S and the cuff misalignment angle ω was created. This model demonstrated the values of S and ω expected for up to 5 cm of joint misalignment. It should be noted that 5 cm of joint misalignment is likely an extreme case and is not expected during regular operation.

Apart from being a novel device, this shoulder exoskeleton could be utilized for either rehabilitation or augmentation. In its current keyboard control setup, it could be used for forms of upper limb rehabilitation that are sensitive to the effects of joint misalignment. In regard to assistive applications, this device could be mounted to an electric wheelchair to help those with upper limb impairments. Another application would be to integrate proximity sensors or piezoelectric foam into the arm cuff in order to allow for a different control method targeted at augmentation for industrial or military purposes.

References

- [1] Merlet, J.-P., 2012, *Parallel Robots*, Vol. 74, Springer Science & Business Media, Dordrecht, The Netherlands.
- [2] Taghirad, H. D., 2013, *Parallel Robots: Mechanics and Control*, CRC Press, Boca Raton, FL.
- [3] Gogu, G., 2008, *Structural Synthesis of Parallel Robots*, Springer, Dordrecht, The Netherlands.
- [4] Khatib, O., 1988, "Augmented Object and Reduced Effective Inertia in Robot Systems," American Control Conference, IEEE, Atlanta, GA, June 15–17, pp. 2140–2147.
- [5] Gupta, A., O'Malley, M. K., Patoglu, V., and Burgar, C., 2008, "Design, Control and Performance of Ricewrist: A Force Feedback Wrist Exoskeleton for Rehabilitation and Training," *Int. J. Rob. Res.*, **27**(2), pp. 233–251.
- [6] Roy, A., Krebs, H. I., Patterson, S. L., Judkins, T. N., Khanna, I., Forrester, L. W., Macko, R. M., and Hogan, N., 2007, "Measurement of Human Ankle Stiffness Using the Anklebot," IEEE 10th International Conference on Rehabilitation Robotics, ICORR 2007, IEEE, Noordwijk, The Netherlands, June 13–15, pp. 356–363.
- [7] Klein, J., Spencer, S., Allington, J., Bobrow, J. E., and Reinkensmeyer, D. J., 2010, "Optimization of a Parallel Shoulder Mechanism to Achieve a High-Force, Low-Mass, Robotic-Arm Exoskeleton," *IEEE Trans. Rob.*, **26**(4), pp. 710–715.
- [8] Veeger, H., 2000, "The Position of the Rotation Center of the Glenohumeral Joint," *J. Biomech.*, **33**(12), pp. 1711–1715.
- [9] Harryman, D. T., Sidles, J., Clark, J. M., McQuade, K. J., Gibb, T. D., and Matzen, F. A., 1990, "Translation of the Humeral Head on the Glenoid With Passive Glenohumeral Motion," *J. Bone Jt. Surg. Am.*, **72**(9), pp. 1334–1343.
- [10] Haninger, K., Lu, J., Chen, W., and Tomizuka, M., 2014, "Kinematic Design and Analysis for a Macaque Upper-Limb Exoskeleton With Shoulder Joint Alignment," 2014 IEEE/RSJ International Conference on Intelligent Robots and Systems (IROS 2014), Chicago, IL, Sept. 14–18, pp. 478–483.
- [11] Carignan, C., Liszka, M., and Roderick, S., 2005, "Design of an Arm Exoskeleton With Scapula Motion for Shoulder Rehabilitation," 12th International Conference on Advanced Robotics, ICAR'05, IEEE, Seattle, WA, July 18–20, pp. 524–531.
- [12] Jung, Y., and Bae, J., 2014, "Performance Verification of a Kinematic Prototype 5-DOF Upper-Limb Exoskeleton With a Tilted and Vertically Translating Shoulder Joint," 2014 IEEE/ASME International Conference on Advanced Intelligent Mechatronics (AIM), Besancon, France, July 8–11, pp. 263–268.
- [13] Mihelj, M., Nef, T., and Riener, R., 2007, "Armin II-7 DOF Rehabilitation Robot: Mechanics and Kinematics," 2007 IEEE International Conference on Robotics and Automation, Rome, Italy, Apr. 10–14, pp. 4120–4125.
- [14] Schiele, A., and Visentin, G., 2003, "The ESA Human Arm Exoskeleton for Space Robotics Telepresence," 7th International Symposium on Artificial Intelligence, Robotics and Automation in Space, Nara, Japan, May 19–23, pp. 19–23.
- [15] Gao, X.-S., Lei, D., Liao, Q., and Zhang, G.-F., 2005, "Generalized Stewart-Gough Platforms and Their Direct Kinematics," *IEEE Trans. Rob.*, **21**(2), pp. 141–151.
- [16] Jiang, Q., and Gosselin, C. M., 2009, "Determination of the Maximal Singularity-Free Orientation Workspace for the Gough–Stewart Platform," *Mech. Mach. Theory*, **44**(6), pp. 1281–1293.
- [17] Dasgupta, B., and Mruthyunjaya, T., 2000, "The Stewart Platform Manipulator: A Review," *Mech. Mach. Theory*, **35**(1), pp. 15–40.
- [18] Pons, J. L., 2010, "Rehabilitation Exoskeletal Robotics," *IEEE Eng. Med. Biol. Mag.*, **29**(3), pp. 57–63.
- [19] Jarrassé, N., and Morel, G., 2012, "Connecting a Human Limb to an Exoskeleton," *IEEE Trans. Rob.*, **28**(3), pp. 697–709.
- [20] Vitiello, N., Lenzi, T., Roccella, S., De Rossi, S. M., Cattin, E., Giovacchini, F., Vecchi, F., and Carrozza, M., 2013, "Neuroexos: A Powered Elbow Exoskeleton for Physical Rehabilitation," *IEEE Trans. Rob.*, **29**(1), pp. 220–235.
- [21] Cempini, M., De Rossi, S. M., Lenzi, T., Vitiello, N., and Carrozza, M., 2013, "Self-Alignment Mechanisms for Assistive Wearable Robots: A Kinostatic Compatibility Method," *IEEE Trans. Rob.*, **29**(1), pp. 236–250.
- [22] Gan, D., Dai, J. S., Dias, J., and Seneviratne, L., 2015, "Forward Kinematics Solution Distribution and Analytic Singularity-Free Workspace of Linear-Actuated Symmetrical Spherical Parallel Manipulators," *ASME J. Mech. Rob.*, **7**(4), p. 041007.
- [23] Tao, Z., and An, Q., 2013, "Interference Analysis and Workspace Optimization of 3-RRR Spherical Parallel Mechanism," *Mech. Mach. Theory*, **69**, pp. 62–72.
- [24] Di Gregorio, R., 2003, "Kinematics of the 3-UPU Wrist," *Mech. Mach. Theory*, **38**(3), pp. 253–263.
- [25] Saltaren, R. J., Sabater, J. M., Yime, E., Azorin, J. M., Aracil, R., and Garcia, N., 2007, "Performance Evaluation of Spherical Parallel Platforms for Humanoid Robots," *Robotica*, **25**(03), pp. 257–267.
- [26] Walter, D. R., Husty, M. L., and Pfurner, M., 2009, "A Complete Kinematic Analysis of the SNU 3-UPU Parallel Robot," *Contemp. Math.*, **496**, pp. 331–347.